IEEE Access
Multidisciplinary | Rapid Review | Open Access Journal

Received September 25, 2020, accepted October 12, 2020, date of publication October 19, 2020, date of current version October 27, 2020.

Digital Object Identifier 10.1109/ACCESS.2020.3032139

On Performance Analysis of NOMA-Aided Hybrid Satellite Terrestrial Relay With Application in Small-Cell Network

NGOC-LONG NGUYEN[1], HONG-NHU NGUYEN[1], ANH-TU LE[2], DINH-THUAN DO[3], (Senior Member, IEEE), AND MIROSLAV VOZNAK[1], (Senior Member, IEEE)

[1]Department of Telecommunications, VSB Technical University of Ostrava, 70833 Ostrava, Czech Republic
[2]Faculty of Electronics Technology, Industrial University of Ho Chi Minh City (IUH), Ho Chi Minh City 700000, Vietnam
[3]Department of Computer Science and Information Engineering, College of Information and Electrical Engineering, Asia University, Taichung 41354, Taiwan

Corresponding author: Dinh-Thuan Do (dodinhthuan@asia.edu.tw)

This work was supported by the Czech Ministry of Education, Youth and Sports conducted at the VSB - Technical University of Ostrava under Grant SP2020/65.

ABSTRACT Satellite communication systems need to be integrated with emerging small-cell network to provide seamless connectivity and high-speed broadband access for mobile users in future wireless networks. In this paper, we study a hybrid satellite-terrestrial relay system (HSTRS) employing small cell transmission under interference constraint with macro-cell users. To characterize such HSTRS-assisted small-cell network, Shadowed-Rician fading for satellite links and Nakagami-*m* fading for terrestrial links are adopted. We further deploy non-orthogonal multiple access (NOMA) to improve spectrum efficiency. To provide performance analysis, we derive exact formulas for outage probability and throughput of the considered HSTRS, and further examine its achievable diversity order. More importantly, we conduct the performance analysis by indicating performance gaps among two users, and such a gap depends on power allocation factors. We evaluate key performance metrics through the derived analytical expressions to provide useful framework of HSTRN and to characterize the impact of interference in different cells, and integer values of the per-hop fading severity parameters. The useful guidelines are introduced in the design of futuristic HSTRS for small-cell communications.

INDEX TERMS Hybrid satellite-terrestrial systems, small-cell, outage probability, Shadowed-Rician fading.

I. INTRODUCTION

In past decades, satellite communication systems are widely deployed in various applications of broadcasting and navigation due to its broad coverage to terrestrial users [1]. Such systems have received considerable attentions from the research community [2], [3]. The transmission of the line of sight (LoS) link between source and a terrestrial destination in such systems is limited by obstacles related to the masking effect. When the satellite elevation's angles are low or the terrestrial user is located indoor, it is reported that worse case caused by effects from obstacles. By exploiting relaying techniques to improve coverage and reliability, the particular work [1] proposed the hybrid satellite-terrestrial relay system (HSTRS) to reduce the masking effect. Presently, the HSTRS benefits to develop integrated technique by combining HSTRS and existing systems. For example, the authors in [4]–[6] presented amplify-and-forward (AF) relaying to improve the performance of HSTRS. While HSTRS has been studied with application of the decode-and-forward (DF) relaying mode [7] and [8]. The authors explored the impact of hardware imperfections on HSTRS, where a geosynchronous earth orbit (GEO) satellite sends its data to the terrestrial destination with the assistance of DF-aided terrestrial relays [9]. They derived expressions of the outage performance. The authors in [10] evaluated the delay-limited throughput of a HSTRS in hybrid automatic repeat request (HARQ) mode. In their system model, a satellite communicates with a user under the scenario of an AF terrestrial relay. Particularly, they provided the mathematical analysis for two cases, i.e.

The associate editor coordinating the review of this manuscript and approving it for publication was Peng-Yong Kong.

the fixed gain AF relaying and the channel state information (CSI)-assisted protocols [10]. Sharma *et al.* [11] investigated a HSTRS where multiple DF three-dimensional (3-D) mobile unmanned aerial vehicle (UAV) relays assist a satellite to send information to a ground user equipment (UE). In other work, the secure performance at physical layer in a hybrid satellite and free-space optical (FSO) cooperative system is studied [12]. They derived exact analytical formula together with the asymptotic analysis for the average secrecy capacity and secrecy outage probability (SOP) for both cases of AF and DF relaying. However, the studies in [6]- [12] only considered hybrid terrestrial-satellite applied in traditional cellular networks. It is noted that the performance of such systems is inherently low due to the inefficient use for massive connections and higher coverage area.

To overcome above difficulties, the non-orthogonal multiple access (NOMA) techniques have recently been proposed and applied to HSTRS [13]–[19]. In principle, NOMA systems studied in [13]–[15] allow multiple users to share the same resource such as the frequency, time, space, or code domain. The other benefits of NOMA include massive connectivity, high spectral efficiency and low delay. For example, considering as attractive attribute of NOMA, the requirements of fairness and spectrum efficiency can be satisfied by cognitive radio transmission [15]. In [16], the security and the reliability of the ambient backscatter (AmBC) NOMA systems are studied, where the base station is able to send information to two NOMA users while an eavesdropper still overhears main signal. In [17], [18] the benefits of unmanned aerial vehicle (UAV) are found in UAV-NOMA. Specifically, in multi-way relaying NOMA networks, multiple terrestrial users aim to communicate their mutual signals by enabling AF-aided UAV relay [18]. Further, [18] considered real situation of the residual hardware impairments (RHIs) at the transceivers. There exists some works integrating NOMA with HSTRNs [19]–[23]. The authors in [19] applied a user with better channel condition as a relay node and forwards signal to other users, thus alleviating the masking effect of users with poor channel conditions in heavy shadowing. The authors in [21] and [22] introduced NOMA to cognitive radio-based HSTRNs, which permits spectrum sharing in the manner of the underlay mode. The authors in [21] studied NOMA based HSTRN using cooperative transmission. Reference [21] and [22] extended previous works to architecture of spectrum sharing. In particular, they only considered the priority of primary user while the fairness between the primary network and the secondary network did not evaluate. The authors in [23] investigated the performance of an underlay cognitive hybrid satellite-terrestrial network which includes a primary satellite transmitter with corresponding terrestrial receiver while the secondary transmitter (ST) communicates with its paired users on the ground.

In other emerging networks, a promising network architecture is known as the heterogeneous (Hetnet) cellular network. In such Hetnet-based cellular network, a macro cell typically coexists with some kinds of small cells, e.g., pico cells, femto cells and micro cells [24]. In heterogeneous cellular networks, expensive macro base station (MBS) needs assistance of a number of surrounding economical small base stations (SBSs) to expand the network coverage and capacity at a reduced expense [25]. Small-cell approach is better than the conventional macro-centric networks in term of capacity and coverage improvements [26]. Such system becomes an easy and cost-efficient deployment solution. Some other advanced technologies, such as full duplex (FD), caching and massive multiple-input and multiple-out (MIMO), are introduced to facilitate dense deployment of small cell base stations (SBSs) [27]. A small-cell network was studied in the context of Hetnet-based cellular networks for both downlink and uplink by introducing three techniques including full-duplex transmission mode, energy harvesting, and power domain-based NOMA schemes [28]. They derive analytical formula to evaluate the system's performance in terms of the outage probability and throughput.

A. RELATED WORK AND MOTIVATIONS

The authors in [29] investigated a cooperative small-cell system containing M small-cell transmitters and N relays to exhibit the outage performance of opportunistic relaying scheme. A renewable energy-based resource allocation method was proposed for full-duplex small-cell networks [30]. They presented method namely an outage-aware power allocation scheme which is considered as an optimal transmission strategy for a two-way transmission between a base station and user equipment in one single small-cell network. Reference [31] explored a sleeping scheme in the 5G small-cell networks by enabling energy harvesting function. In addition, the cooperative caching and the energy consumption minimization problem are considered.

To our best knowledge, recent work has not yet analyzed the performance of a small-cell HSTRS with the enabler of NOMA. This motivates us to study small-cell HSTRS relying on NOMA. Note that such a configuration can boost the performance of HSTRS, especially with extended coverage under bottleneck link behavior of traditional communications.

B. OUR CONTRIBUTION

Particularly, our main contributions can be outlined as follows:

- We propose a small-cell HSTRS relying on NOMA and main analysis is based on system performance of small-cell users. The DF protocol adopted in relay to forward signals to improve performance of cell-edge users in the coverage of small-cell. We deploy the Shadowed-Rician fading model for the pertinent satellite links and Nakagami-m faded channels model for the terrestrial links of the considered small-cell network.
- The normal operation of small-cell network can achieved by satisfying the criterion for minimal impacts on performance of the macro-cell network network, and eventually, interference management between

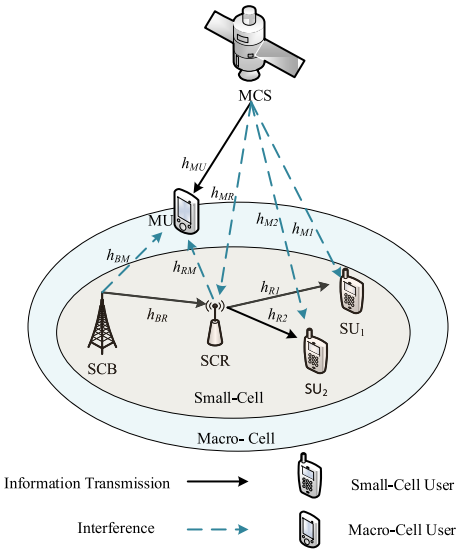

FIGURE 1. System model of small-cell HSTRS relying on NOMA.

macro-cell and small-cell networks are guaranteed. To provide performance analysis, we first characterize the end-to-end signal-to-noise ratios (SNRs), then the closed-form expressions of the outage probability (OP) are derived for the two small-cell users. Hereby, we explore main factors affecting to performance gap among two small-cell users such as power allocation strategy applied to two such users.

- To look at the diversity performance of the considered network, we further derive the asymptotic behavior of the derived formula of OP. In addition, we explore system performance in terms of both heavy shadowing (HS) and average shadowing (AS) scenarios related to the satellite links. As a result, more insights are provided to highlight the system performance.

The rest of this paper is summarized as follows. In Section II, we elaborate the structure of small-cell HSTRS relying on NOMA, then we compute the end-to-end SNRs over considered channels. We characterize the satellite and terrestrial channels and analyze the OP performance of such small-cell network in Section III. Section IV provides the numerical and simulation results, and finally the conclusion is conducted in Section V.

II. SYSTEM MODEL

In this paper, a small-cell base station (SCB), a small-cell relay (SCR) and two small-cell user $SU_i (i \in \{1, 2\})$ are considered to implement the advantage of NOMA, i.e. higher spectrum efficiency.[1] Furthermore, the small-cell network can be operated together with a macro-cell satellite (MCS) serving macro-cell users (MUs).

The transmit power at the SCB and the SCR in the context of small-cell is limited by many factors [32]. These

[1]We limit our analysis to two-user model as the literature [19]- [21]. Similar analysis can be performed for the case of higher number of users.

TABLE 1. The main denotations in the system model.

Symbol	Description
h_{SR}	The channel coefficient between the small-cell base station and relay
h_{SM}	The channel coefficient between the small-cell base station and the macro-cell user
h_{RM}	The channel coefficient between the small-cell relay and the macro-cell user
h_{MU}	The channel coefficient between the macro-cell satellite and user
h_{MR}	The channel coefficient of the interference link between the macro-cell satellite and the small-cell relay
h_{Mi}	The channel coefficient of the interference link between the macro-cell satellite and the small-cell user SU_i
h_{Ri}	The channel coefficient between the small-cell relay and user U_i
$P_{SCB}, \bar{P}_{SCB}$	The transmit power and maximum transmit power at SCQ, respectively
P_M	The interference temperature constraint at macro-cell user
P_{MCS}	The transmit power at macro-cell satellite
x_i	The information symbol of small-cell user SU_i
x_M	The information symbol for macro-cell user
Φ_i	The power allocation factors with $\Phi_1 > \Phi_2$ and $\Phi_1 + \Phi_2 = 1$
n_{SCR}, n_{SU_i}	The additive white Gaussian noise with $\mathcal{CN}(0, N_0)$

factors partly depend on channels. In particular, we denote $\psi = \frac{1}{|h_{QM}|^2}$, then we have the transmit power at the SCB and the SCR are given by

$$P_{SCQ} = \min\left(\bar{P}_{SCQ}, P_M \psi\right), \quad Q \in \{B, R\}. \tag{1}$$

In the first phase, the received signal at the SCR is formulated by

$$y_{SCR} = h_{BR}\sqrt{P_{SCB}}\left(\sqrt{\Phi_1}x_1 + \sqrt{\Phi_2}x_2\right) + \sqrt{P_{MCS}}h_{MR}x_M + n_{SCR}. \tag{2}$$

To evaluate system metric, it need be computed the signal-to-interference- plus-noise ratio (SINR) at the SCR to detect signal x_1. In particular, SINR is given by

$$\Gamma_{SCR\to x_1} = \frac{P_{SCB}|h_{BR}|^2 \Phi_1}{P_{SCB}|h_{BR}|^2 \Phi_2 + P_{MCS}|h_{MR}|^2 + N_0}. \tag{3}$$

By employing SIC, the SINR to detect x_2 at the SCR is given by

$$\Gamma_{SCR\to x_2} = \frac{P_{SCB}|h_{BR}|^2 \Phi_2}{P_{MCS}|h_{MR}|^2 + N_0}. \tag{4}$$

In the second phase, the relay SCR transmits signal to the cell-edge users SU_i. The received signal at SU_i is given by

$$y_{SU_i} = h_{Ri}\sqrt{P_{SCR}}\left(\sqrt{\Phi_1}x_1 + \sqrt{\Phi_2}x_2\right) + \sqrt{P_{MCS}}h_{Mi}x_M + n_{SU_i}. \tag{5}$$

The SINR measured at the SU_1 to detect signal x_1 is given by

$$\Gamma_{SU_1\to x_1} = \frac{P_{SCR}|h_{R1}|^2 \Phi_1}{P_{SCR}|h_{R1}|^2 \Phi_2 + P_{MCS}|h_{M1}|^2 + N_0}. \tag{6}$$

Then, the SINR at SU_2 for detecting of signal x_1 is expressed by

$$\Gamma_{SU_2\to x_1} = \frac{P_{SCR}\left|h_{R2}\right|^2 \Phi_1}{P_{SCR}\left|h_{R2}\right|^2 \Phi_2 + P_{MCS}\left|h_{M2}\right|^2 + N_0}. \quad (7)$$

The user SU_2 benefits by SIC, then SINR to detect signal x_2 at SU_2 is given by

$$\Gamma_{SU_2\to x_2} = \frac{P_{SCR}\left|h_{R2}\right|^2 \Phi_2}{P_{MCS}\left|h_{M2}\right|^2 + N_0}. \quad (8)$$

In next section, we focus on main metric, outage probability (OP) and then throughput in delay-limited transmission mode is also provided. These metrics play important role in design relevant equipment for the considered system.

III. PERFORMANCE ANALYSIS

A. CHANNEL MODELS

We adopt Shadowed-Rician fading model for the satellite links. In particular, the probability density function of $|h_{Mj}|^2$ with $j \in (R, 1, 2)$ is formulated by [4]

$$f_{|h_{Mj}|^2}(x) = \alpha_{Mj} e^{-\beta_{Mj}x}\, {}_1F_1\left(m_{Mj}; 1; \delta_{Mj}x\right), \quad x > 0, \quad (9)$$

where $\alpha_{Mj} = \left(\frac{2b_{Mj}m_{Mj}}{2b_{Mj}m_{Mj}+\Omega_{Mj}}\right)^{m_{Mj}}/2b_{Mj}$, $\beta_{Mj} = 0.5b_{Mj}$ and $\delta_{Mj} = \Omega_{Mj}/\left(2b_{Mj}\right)\left(2b_{Mj}m_{Mj}+\Omega_{Mj}\right)$, with Ω_{Mj} and $2b_{Mj}$ represents the respective average power of the LOS and multi-path components, m_{Mj} is the fading severity parameter and ${}_1F_1(.)$ is the confluent hypergeometric function of the first kind [37, Eq. 9.210.1].

In this paper, we consider arbitrary integer-valued fading severity parameter [33]. Then, we can simplify (9) as

$$f_{|h_{Mj}|^2}(x) = \alpha_{Mj} \sum_{n_{Mj}=0}^{m_{Mj}-1} \zeta_{Mj}\left(n_{Mj}\right) x^{n_{Mj}} e^{-\Psi_{Mj}x}, \quad (10)$$

where $\zeta_{Mi}\left(n_{Mj}\right) = (-1)^{n_{Mj}}\left(1-m_{Mj}\right)_{n_{Mj}}\delta_{Mj}^{n_{Mj}}/\left(n_{Mj}!\right)^2$, $(.)_a$ is the Pochhammer symbol [37, p.xliii] and $\Psi_{Mi} = \beta_{Mi} - \delta_{Mi}$. Thus, the cumulative distribution function (CDF) of $|h_{Mj}|^2$ is expressed by

$$F_{|h_{Mj}|^2}(x) = 1 - \alpha_{Mj} \sum_{n_{Mj}=0}^{m_{Mj}-1} \zeta_{Mj}\left(n_{Mj}\right) \times \sum_{q=0}^{n_{Mj}} \frac{n_{Mj}!}{q!\left(\Psi_{Mj}\right)^{n_{Mj}-q+1}} x^q e^{-\Psi_{Mi}x}. \quad (11)$$

The probability density function (PDF) and CDF of $|h_k|^2$ for $k \in \{BR, BM, RM, R1, R2\}$ are given respectively as

$$f_{|h_k|^2}(x) = \frac{x^{m_k-1}}{\Gamma(m_k)\,\omega_k^{m_k}} e^{-\frac{x}{\omega_k}}, \quad (12)$$

and

$$F_{|h_k|^2}(x) = \frac{\gamma(m_k, x/\omega_k)}{\Gamma(m_k)} = 1 - e^{-\frac{x}{\omega_k}} \sum_{n_k=0}^{m_k-1} \frac{x^{n_k}}{\omega_k^{n_k} n_k!}. \quad (13)$$

where $\omega_k = \frac{\lambda_k}{m_k}$, m_k and λ_k denotes the fading severity and average power, respectively.

B. OUTAGE PERFORMANCE

1) OUTAGE PERFORMANCE OF SU_1

To evaluate how the two edge-users work in the context of small-cell, we continue to look at the OP performance. The user SU_1 need to detect its signal x_1. Based on conditions related to such outage event, the OP of user SU_1 is formulated by

$$\begin{aligned}\mathcal{P}_{x_1} &= 1 - \Pr\left(\min\left(\Gamma_{SCR\to x_1}, \Gamma_{SU_1\to x_1}, \Gamma_{SU_2\to x_1}\right) > \gamma_1\right) \\ &= 1 - \underbrace{\Pr\left(\Gamma_{SCR\to x_1} > \gamma_1\right)}_{A_1} \\ &\quad \times \underbrace{\Pr\left(\Gamma_{SU_1\to x_1} > \gamma_1\right)}_{A_2} \underbrace{\Pr\left(\Gamma_{SU_2\to x_1} > \gamma_1\right)}_{A_3}, \end{aligned} \quad (14)$$

where $\gamma_i = 2^{2R_i} - 1$ is the threshold SNR corresponding to target rates R_i for two users; R_i as the target rate of user SU_i.

Proposition 1: As a part of such OP, term A_1 can be expressed as (15), shown at the bottom of the next page.

Proof: See Appendix A

In term of computing of A_2, substituting (6) into (14), we have

$$\begin{aligned} A_2 &= \Pr\left(|h_{R1}|^2 > \frac{\theta_1\left(\rho_S|h_{M1}|^2+1\right)}{\bar{\rho}_R}, \bar{\rho}_R < \frac{\rho_M}{|h_{RM}|^2}\right) \\ &\quad + \Pr\left(|h_{R1}|^2 > \frac{\theta_1|h_{RM}|^2\left(\rho_S|h_{M1}|^2+1\right)}{\rho_M}, \bar{\rho}_R > \frac{\rho_M}{|h_{RM}|^2}\right). \end{aligned} \quad (16)$$

Similarly, A_2 can be calculated by

$$\begin{aligned} A_2 &= \sum_{n_{M1}=0}^{m_{M1}-1}\sum_{n_{R1}=0}^{m_{R1}-1}\sum_{b=0}^{n_{R1}} \binom{n_{R1}}{b} \frac{\zeta_{M1}(n_{M1})(n_{M1}+b)!\alpha_{M1}}{n_{R1}!\Gamma(m_{RM})} \\ &\quad \times \left(\frac{(\omega_{R1}\bar{\rho}_R)^{n_{MR}-n_{R1}+b+1}\,\gamma\left(m_{RM}, \rho_M/\omega_{RM}\bar{\rho}_R\right) e^{-\frac{\theta_1}{\bar{\rho}_B\omega_{R1}}}}{\rho_S^{-b}\theta_1^{-n_{R1}}\left(\theta_1\rho_S + \Psi_{M1}\bar{\rho}_R\omega_{R1}\right)^{n_{MR}+b+1}} \right. \\ &\quad \left. + \frac{\rho_S^b\theta_1^{n_{R1}}\omega_{RM}^{n_{R1}}\Psi_{M1}^{-n_{M1}-b-1}\left(\rho_M\omega_{R1}\right)^{m_{RM}}}{\Gamma(n_{M1}+b+1)\left(\theta_1\omega_{RM}+\omega_{R1}\rho_M\right)^{m_{RM}+n_{R1}}} \right) \\ &\quad \times G_{1,[1:1],0,[1:1]}^{1,1,1,1,0} \left[\frac{\frac{\theta_1\rho_S\omega_{RM}}{\Psi_{M1}\left(\theta_1\omega_{RM}+\omega_{R1}\rho_M\right)}}{\frac{\omega_{R1}\omega_{RM}\bar{\rho}_R}{\theta_1\omega_{RM}+\omega_{R1}\rho_M}} \middle| \begin{matrix} 1+m_{RM}+n_{R1} \\ -n_{M1}-b;\,1 \\ -- \\ 0;\,0 \end{matrix} \right]. \end{aligned} \quad (17)$$

Moreover, we can write A_3 as

$$\begin{aligned}A_3 &= \sum_{n_{M2}=0}^{m_{M2}-1}\sum_{n_{R2}=0}^{m_{R2}-1}\sum_{c=0}^{n_{R2}}\binom{n_{R2}}{c}\frac{\zeta_{M2}\left(n_{M2}\right)\left(n_{M2}+c\right)!\alpha_{M2}}{n_{R2}!\Gamma\left(m_{RM}\right)}\\ &\times\left(\frac{\left(\omega_{R2}\bar{\rho}_R\right)^{n_{MR}-n_{R2}+c+1}\gamma\left(m_{RM},\rho_M/\omega_{RM}\bar{\rho}_R\right)e^{-\frac{\theta_1}{\bar{\rho}_B\omega_{R2}}}}{\rho_S^{-C}\theta_1^{-n_{R2}}\left(\theta_1\rho_S+\Psi_{M2}\bar{\rho}_R\omega_{R2}\right)^{n_{MR}+c+1}}\right.\\ &+\frac{\rho_S^b\theta_1^{n_{R2}}\omega_{RM}^{n_{R2}}\Psi_{M2}^{-n_{M2}-c-1}\left(\rho_M\omega_{R2}\right)^{m_{RM}}}{\Gamma\left(n_{M2}+c+1\right)\left(\theta_1\omega_{RM}+\omega_{R2}\rho_M\right)^{m_{RM}+n_{R2}}}\\ &\times G_{1,[1:1],0,[1:1]}^{1,1,1,1,0}\\ &\left.\times\left[\begin{array}{c|c}\frac{\theta_1\rho_S\omega_{RM}}{\Psi_{M2}\left(\theta_1\omega_{RM}+\omega_{R2}\rho_M\right)} & 1+m_{RM}+n_{R1}\\ \frac{\omega_{R2}\omega_{RM}\bar{\rho}_R}{\theta_1\omega_{RM}+\omega_{R2}\rho_M} & -n_{M2}-c;\,1\\ & --\\ & 0;\,0\end{array}\right]\right).\end{aligned}\tag{18}$$

Finally, the closed-form expression of OP for user SU_1 can be obtained as below

$$\mathcal{P}_{x_1}=\begin{cases}1-A_1\times A_2\times A_3, & \text{if}:\gamma_1<\frac{\Phi_1}{\Phi_2}\\ 1 & ,\text{otherwise.}\end{cases}\tag{19}$$

2) OUTAGE PERFORMANCE OF SU_2

Different from performance of SU_1, user SU_2 is able to detect its signal for the first hop and the second hop based on achieved SINR, i.e. $\Gamma_{SCR\to x_2}$, $\Gamma_{SU_2\to x_2}$. In particular, the OP of user SU_2 is formulated by

$$\begin{aligned}\mathcal{P}_{x_2} &= 1-\Pr\left(\min\left(\Gamma_{SCR\to x_2},\Gamma_{SU_2\to x_2}\right)>\gamma_2\right)\\ &= 1-\underbrace{\Pr\left(\Gamma_{SCR\to x_2}>\gamma_2\right)}_{\bar{A}_1}\underbrace{\Pr\left(\Gamma_{SU_2\to x_2}>\gamma_2\right)}_{\bar{A}_2}.\end{aligned}\tag{20}$$

Proposition 2: The first term in (20) can be expressed as

$$\begin{aligned}\bar{A}_1 &= \sum_{n_{MR}=0}^{m_{MR}-1}\sum_{n_{BR}=0}^{m_{BR}-1}\sum_{a=0}^{n_{BR}}\binom{n_{BR}}{a}\frac{\zeta_{MR}\left(n_{MR}\right)\left(n_{MR}+a\right)!\alpha_{MR}}{n_{BR}!\Gamma\left(m_{BM}\right)}\\ &\times\left(\frac{\left(\omega_{BR}\bar{\rho}_B\right)^{n_{MR}-n_{BR}+a+1}\gamma\left(m_{BM},\rho_M/\omega_{BM}\bar{\rho}_B\right)e^{-\frac{\theta_2}{\bar{\rho}_B\omega_{BR}}}}{\rho_S^{-a}\theta_2^{-n_{BR}}\left(\theta_2\rho_S+\Psi_{MR}\bar{\rho}_B\omega_{BR}\right)^{n_{MR}+a+1}}\right.\\ &\left.+\frac{\rho_S^a\theta_2^{n_{BR}}\omega_{BM}^{n_{BR}}\Psi_{MR}^{-n_{MR}-a-1}\left(\rho_M\omega_{BR}\right)^{m_{BM}}}{\Gamma\left(n_{MR}+a+1\right)\left(\theta_2\omega_{BM}+\omega_{BR}\rho_M\right)^{m_{BM}+n_{BR}}}\right.\\ &\times G_{1,[1:1],0,[1:1]}^{1,1,1,1,0}\\ &\left.\times\left[\begin{array}{c|c}\frac{\theta_2\rho_S\omega_{BM}}{\Psi_{MR}\left(\theta_2\omega_{BM}+\omega_{BR}\rho_M\right)} & 1+m_{BM}+n_{BR}\\ \frac{\omega_{BR}\omega_{BM}\bar{\rho}_B}{\theta_2\omega_{BM}+\omega_{BR}\rho_M} & -n_{MR}-a;\,1\\ & --\\ & 0;\,0\end{array}\right]\right).\end{aligned}\tag{21}$$

Proof: With the help of (1) and (4), we can write $\bar{A}_1$ as

$$\begin{aligned}\bar{A}_1 &= \Pr\left(\frac{P_{SCB}\left|h_{BR}\right|^2\Phi_2}{P_{MCS}\left|h_{MR}\right|^2+N_0}>\gamma_2\right)\\ &= \Pr\left(\left|h_{BR}\right|^2>\frac{\theta_2\left(\rho_S\left|h_{MR}\right|^2+1\right)}{\bar{\rho}_B},\bar{\rho}_B<\frac{\rho_M}{\left|h_{BM}\right|^2}\right)\\ &+\Pr\left(\left|h_{BR}\right|^2>\frac{\theta_2\left|h_{BM}\right|^2\left(\rho_S\left|h_{MR}\right|^2+1\right)}{\rho_M},\bar{\rho}_B>\frac{\rho_M}{\left|h_{BM}\right|^2}\right),\end{aligned}\tag{22}$$

where $\theta_2=\frac{\gamma_2}{\Phi_2}$. Similarly appendix A, the closed-form expression of $\bar{A}_1$ can be obtained.

The proof is completed.

Similarly, $\bar{A}_2$ is given as

$$\begin{aligned}\bar{A}_2 &= \sum_{n_{M2}=0}^{m_{M2}-1}\sum_{n_{R2}=0}^{m_{R2}-1}\sum_{c=0}^{n_{R2}}\binom{n_{R2}}{c}\frac{\zeta_{M2}\left(n_{M2}\right)\left(n_{M2}+c\right)!\alpha_{M2}}{n_{R2}!\Gamma\left(m_{RM}\right)}\\ &\times\left(\frac{\left(\omega_{R2}\bar{\rho}_R\right)^{n_{MR}-n_{R2}+c+1}\gamma\left(m_{RM},\rho_M/\omega_{RM}\bar{\rho}_R\right)e^{-\frac{\theta_2}{\bar{\rho}_B\omega_{R2}}}}{\rho_S^{-C}\theta_2^{-n_{R2}}\left(\theta_2\rho_S+\Psi_{M2}\bar{\rho}_R\omega_{R2}\right)^{n_{MR}+c+1}}\right.\\ &+\frac{\rho_S^b\theta_2^{n_{R2}}\omega_{RM}^{n_{R2}}\Psi_{M2}^{-n_{M2}-c-1}\left(\rho_M\omega_{R2}\right)^{m_{RM}}}{\Gamma\left(n_{M2}+c+1\right)\left(\theta_2\omega_{RM}+\omega_{R2}\rho_M\right)^{m_{RM}+n_{R2}}}\\ &\times G_{1,[1:1],0,[1:1]}^{1,1,1,1,0}\\ &\left.\times\left[\begin{array}{c|c}\frac{\theta_2\rho_S\omega_{RM}}{\Psi_{M2}\left(\theta_2\omega_{RM}+\omega_{R2}\rho_M\right)} & 1+m_{RM}+n_{R1}\\ \frac{\omega_{R2}\omega_{RM}\bar{\rho}_R}{\theta_2\omega_{RM}+\omega_{R2}\rho_M} & -n_{M2}-c;\,1\\ & --\\ & 0;\,0\end{array}\right]\right).\end{aligned}\tag{23}$$

Thus, the closed-form expression of OP for user SU_2 is obtained by

$$\mathcal{P}_{x_2}=1-\bar{A}_1\times\bar{A}_2.\tag{24}$$

Remark 1: In this section, we provide our analytical result on OP. Although, these expressions of OP are complicated,

$$\begin{aligned}A_1 &= \sum_{n_{MR}=0}^{m_{MR}-1}\sum_{n_{BR}=0}^{m_{BR}-1}\sum_{a=0}^{n_{BR}}\binom{n_{BR}}{a}\frac{\zeta_{MR}\left(n_{MR}\right)\left(n_{MR}+a\right)!\rho_S^a\alpha_{MR}\theta_1^{n_{BR}}}{n_{BR}!\Gamma\left(m_{BM}\right)}\left(\frac{\left(\omega_{BR}\bar{\rho}_B\right)^{n_{MR}-n_{BR}+a+1}\gamma\left(m_{BM},\rho_M/\omega_{BM}\bar{\rho}_B\right)e^{-\frac{\theta_1}{\bar{\rho}_B\omega_{BR}}}}{\left(\theta_1\rho_S+\Psi_{MR}\bar{\rho}_B\omega_{BR}\right)^{n_{MR}+a+1}}\right.\\ &\left.+\frac{\omega_{BM}^{n_{BR}}\Psi_{MR}^{-n_{MR}-a-1}\left(\rho_M\omega_{BR}\right)^{m_{BM}}}{\Gamma\left(n_{MR}+a+1\right)\left(\theta_1\omega_{BM}+\omega_{BR}\rho_M\right)^{m_{BM}+n_{BR}}}G_{1,[1:1],0,[1:1]}^{1,1,1,1,0}\left[\begin{array}{c|c}\frac{\theta_1\rho_S\omega_{BM}}{\Psi_{MR}\left(\theta_1\omega_{BM}+\omega_{BR}\rho_M\right)} & 1+m_{BM}+n_{BR}\\ \frac{\omega_{BR}\omega_{BM}\bar{\rho}_B}{\theta_1\omega_{BM}+\omega_{BR}\rho_M} & -n_{MR}-a;\,1\\ & --\\ & 0;\,0\end{array}\right]\right).\end{aligned}\tag{15}$$

TABLE 2. Channel parameters related to the satellite.

Shadowing	b	m	Ω
The heavy shadowing (HS)	0.063	1	0.0007
The average shadowing (AS)	0.251	5	0.279

TABLE 3. Table of main parameters in simulation.

Monte Carlo simulations	10^6 iterations
Power allocation factors	$\Phi_1 = 0.8$ and $\Phi_2 = 0.2$
The target rates	$R_1 = 1, R_2 = 0.5$ bit per channel use (BPCU)
Average power	$\lambda_{BM} = \lambda_{RM} = 0.01$, $\lambda_{BR} = \lambda_{R1} = \lambda_{R2} = 1$
The fading severity	$m = m_{BR} = m_{BM} = m_{RM} = m_{R1} = m_{R2}$

but main impacts rely on the transmit SNR at he small-cell base station and various fading scenarios. For the considered Shadowed-Rician fading for satellite links and Nakagami-m fading for terrestrial links, we further examine these related parameters in numerical simulations. It is predicted that power allocation factors lead to different performance of two small-cell users.

To obtain more insight in term of the desired OP expressions, one can derive the expression for asymptotic OP for two users. We also obtain the achievable diversity order. Such findings are extra benefits to design of such network in practice.

C. ASYMPTOTIC AND DIVERSITY OUTAGE BEHAVIOR ANALYSIS

In this paper, we examine the peak interference constraint. In particular, P_M is fixed value and only $\bar{P}_{SCQ}$ becomes large in the high SNR region. The asymptotic behaviors of OP for user SU_1 in this case is presented as Proposition 3 below.

Proposition 3: The asymptotic OP of SU_1 can be expressed as (25), shown at the bottom of the next bottom page.

Proof: See Appendix B.

Similar to the derivation reported in appendix B, the asymptotic of OP for user SU_2 can be obtained as (26), shown at the bottom of the next bottom page.

Regarding the diversity order, we have such formula

$$\mathcal{D} = -\lim_{\bar{\rho}\to\infty} \frac{\log_{10}\left(\mathcal{P}_{x_i}(\bar{\rho})\right)}{\log_{10}(\bar{\rho})}, \tag{27}$$

It can be concluded that when SNR is larger, the diversity order is zero. We further check this result in numerical simulation section. It is useful insights in design of practical system.

D. THROUGHPUT PERFORMANCE

It is necessary to consider other metric of such system. In particular, the overall throughput can be achieved based on obtained OP derived for performance evaluation of two users. In delay-limited mode, at fixed target rates R_1, R_2 the throughput can be obtained.

According to obtained OPs, we can calculate the overall throughput as

$$\mathcal{T}_{total} = \left(1 - \mathcal{P}_{x_1}\right) R_1 + \left(1 - \mathcal{P}_{x_2}\right) R_2. \tag{28}$$

IV. NUMERICAL RESULTS

To provide mathematical analysis, it is necessary to simulate and illustrate for the proposed small-cell HSTRN relying on NOMA scheme. According main configuration, we set the shadowing scenarios of the satellite links h_{Pj}, including the heavy shadowing (HS) and average shadowing (AS) in Table 2 [35]. We further set $\bar{\rho} = \bar{\rho}_B = \bar{\rho}_R$ and the parameters in Table 3. Moreover, we vary $m = 1$ for the Nakagami-m fading related to terrestrial links. In these following figures, Monte-Carlo simulations are performed to validate the analytical results.

Fig. 2 and Fig. 3 plot the OPs of two users in the considered HSTRS versus the transmit SNR at the MCB $\bar{\rho}$ and the transmit SNR at the SCB ρ_M, respectively. It is valuable result as analytical and Monte-Carlo curves are matched very tightly and it confirms the exactness of derived OP in this paper. It is clearly seen that the OP performance would be improved at high SNR region. The performance gap among two users is resulted by different power allocation factors. More specifically, the OP performance of SU_2 is better than that of SU_1 and two OPs of two users are still better than that of the OMA-based HSTRS. The reason is that the OMA-based HSTRS needs more time slots to transmit two consecutive signals x_1, x_2 while only one time slot is served for NOMA-based HSTRS counterpart. Moreover, the asymptotic curves of OP is matched with the exact OP curves at high SNR regime. It is further confirmed that OP will be unchanged at high SNR. Such situation is consistent with diversity order found in previous section. In Fig. 3, similar trends of OP can be seen.

In Fig. 4, we can see the impact of ρ_S on the OP performance of small-cell network. It can be explained that higher transmit power at MCB leads to limit the transmit power at SCB, then OP will reduce. The other trend of these OPs can be seen similarly with Fig. 2 and Fig. 3. In this experiment, $\rho_S = 5$ exhibits the best performance of small-cell network in term of OP.

Fig. 5 illustrates the OPs of the two users as varying average SNR at SCB from 0 to 50, where the satellite link undergoes HS case. Three cases of channel coefficients are $m = 1, 2, 3$. The performance gap is still seen for these curves related OPs of two users. It is reported that the OPs of two users are best case as $m = 3$. It is obvious to conclude that the improved channels result in better OP performance.

Fig. 6 depicts the OPs of the two users against two crucial parameters, i.e., status of satellite links (HS or AF cases) and the transmit SNR at the SCB $\bar{\rho}$. From the figure, the OPs of two users in the case of HS are better that of AS. At the considered range of the transmit SNR at the SCB $\bar{\rho}$, performance gaps of two users in cases of HS and AS are similar. It is concluded that such OP depends on $\bar{\rho}$ and power allocation

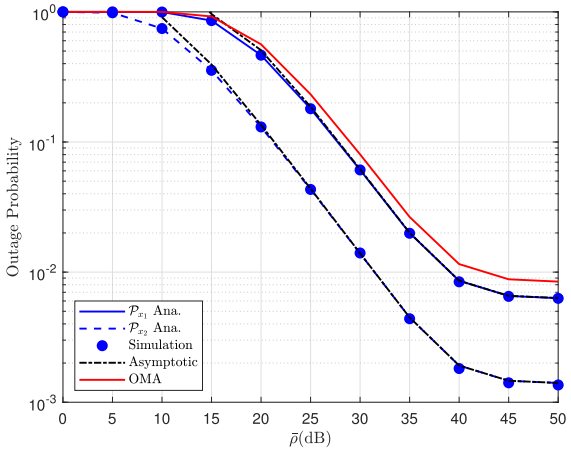

FIGURE 2. The outage probability versus $\bar{\rho}$, where $m = 1$, $\rho_M = 20dB$, $\rho_S = 5dB$ and the satellite link is set HS case.

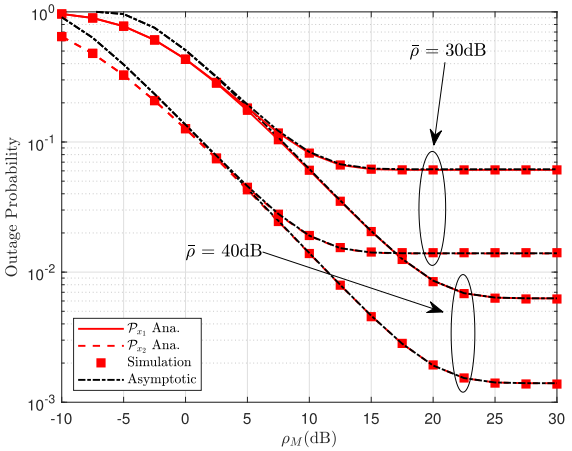

FIGURE 3. The outage probability versus ρ_M, with different values of $\bar{\rho}$, where $m = 1$, $\rho_S = 5dB$ and the satellite link is set HS case.

factors rather than on the specific parameters of satellite links (HS or AS).

Fig. 7 continues to confirm power allocation scheme affecting the OPs of two users. It is worth noting that the OP of user SU_1 depends mainly on Φ_1. In particular, when we increase Φ_1 from 0.5 to 1, the OP performance of user SU_1 improve significantly. In the contrast, the OP performance of SU_2 is definitely better than that of SU_2 at the point of $\Phi_1 = 0.5$, but such OP becomes worse afterward. The main reason is that Φ_1 plays important role in varying value of SINRs, then the corresponding OPs will be changed.

Fig. 8 further provides the curves of the total throughput versus the transmit SNR at SCB $\bar{\rho}$, i.e. throughput for case $R_1 = R_2 = 0.5$. It is clear from (28) that higher fixed target

$$\begin{aligned}\mathcal{P}_{x_1}^{\infty} = 1 - &\left(1 - \sum_{n_{MR}=0}^{m_{MR}-1}\sum_{n_{BR}=0}^{m_{BR}} \binom{m_{BR}}{n_{BR}} \frac{\zeta_{MR}\left(n_{MR}\right)\rho_S^{n_{BR}}\alpha_{MR}\left(n_{MR}+n_{BR}\right)!}{\Gamma\left(m_{BR}+1\right)\Gamma\left(m_{BM}\right)\Psi_{MR}^{n_{MR}+n_{BR}+1}} \left(\frac{\theta_1}{\omega_{BR}}\right)^{m_{BR}}\right.\\ &\times\left.\left(\frac{\gamma\left(m_{BM}, \frac{\rho_N}{\bar{\rho}_B\omega_{BM}}\right)}{\bar{\rho}_B^{m_{BR}}} + \Gamma\left(m_{SP}+m_R, \frac{\rho_M}{\bar{\rho}_B\omega_{BM}}\right)\left(\frac{\omega_{BM}}{\rho_M}\right)^{m_{BR}}\right)\right)\\ &\times\prod_{i=1}^{2}\left(1 - \sum_{n_{Mi}=0}^{m_{Mi}-1}\sum_{n_{Ri}=0}^{m_{Ri}} \binom{m_{Ri}}{n_{Ri}} \frac{\zeta_{Mi}\left(n_{Mi}\right)\rho_S^{n_{Ri}}\alpha_{Mi}\left(n_{Mi}+n_{Ri}\right)!}{\Gamma\left(m_{Ri}+1\right)\Gamma\left(m_{RM}\right)\Psi_{Mi}^{n_{Mi}+n_{Ri}+1}} \left(\frac{\theta_1}{\omega_{Ri}}\right)^{m_{Ri}}\right.\\ &\times\left.\left(\frac{\gamma\left(m_{RM}, \frac{\rho_M}{\bar{\rho}_R\omega_{RM}}\right)}{\bar{\rho}_R^{m_R}} + \Gamma\left(m_{RM}+m_{Ri}, \frac{\rho_M}{\bar{\rho}_R\omega_{RM}}\right)\left(\frac{\omega_{RM}}{\rho_M}\right)^{m_{Ri}}\right)\right).\end{aligned} \tag{25}$$

$$\begin{aligned}\mathcal{P}_{x_2}^{\infty} = 1 - &\left(1 - \sum_{n_{MR}=0}^{m_{MR}-1}\sum_{n_{BR}=0}^{m_{BR}} \binom{m_{BR}}{n_{BR}} \frac{\zeta_{MR}\left(n_{MR}\right)\rho_S^{n_{BR}}\alpha_{MR}\left(n_{MR}+n_{BR}\right)!}{\Gamma\left(m_{BR}+1\right)\Gamma\left(m_{BM}\right)\Psi_{MR}^{n_{MR}+n_{BR}+1}} \left(\frac{\theta_2}{\omega_{BR}}\right)^{m_{BR}}\right.\\ &\times\left.\left(\frac{\gamma\left(m_{BM}, \frac{\rho_N}{\bar{\rho}_B\omega_{BM}}\right)}{\bar{\rho}_B^{m_{BR}}} + \Gamma\left(m_{SP}+m_R, \frac{\rho_M}{\bar{\rho}_B\omega_{BM}}\right)\left(\frac{\omega_{BM}}{\rho_M}\right)^{m_{BR}}\right)\right)\\ &\times\left(1 - \sum_{n_{M2}=0}^{m_{M2}-1}\sum_{n_{R2}=0}^{m_{R2}} \binom{m_{R2}}{n_{R2}} \frac{\zeta_{M2}\left(n_{M2}\right)\rho_S^{n_{R2}}\alpha_{M2}\left(n_{M2}+n_{R2}\right)!}{\Gamma\left(m_{R2}+1\right)\Gamma\left(m_{RM}\right)\Psi_{M2}^{n_{M2}+n_{R2}+1}} \left(\frac{\theta_2}{\omega_{R2}}\right)^{m_{R2}}\right.\\ &\times\left.\left(\frac{\gamma\left(m_{RM}, \frac{\rho_M}{\bar{\rho}_R\omega_{RM}}\right)}{\bar{\rho}_R^{m_R}} + \Gamma\left(m_{RM}+m_{R2}, \frac{\rho_M}{\bar{\rho}_R\omega_{RM}}\right)\left(\frac{\omega_{RM}}{\rho_M}\right)^{m_{R2}}\right)\right).\end{aligned} \tag{26}$$

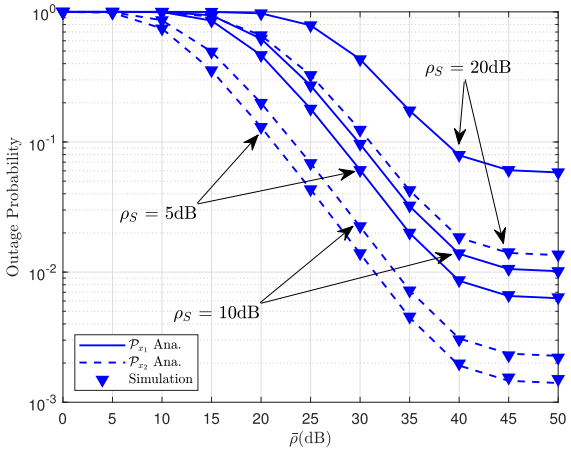

FIGURE 4. The outage probability versus $\bar{\rho}$, with different values of ρ_S, where $m = 1$, $\rho_M = 20dB$ and the satellite link is set HS case.

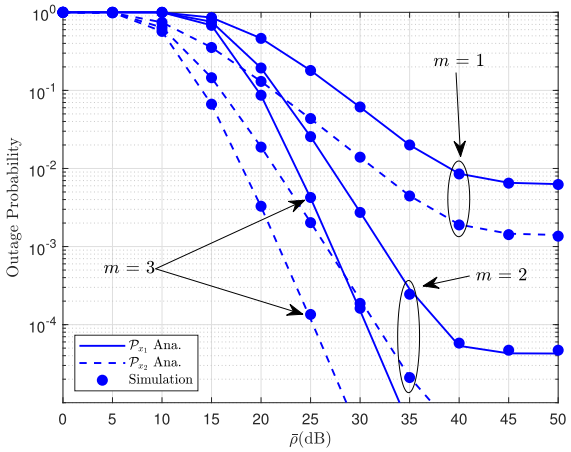

FIGURE 5. The outage probability versus $\bar{\rho}$, with different values of m, where $\rho_M = 20dB$, $\rho_S = 5dB$ and the satellite link is set HS case.

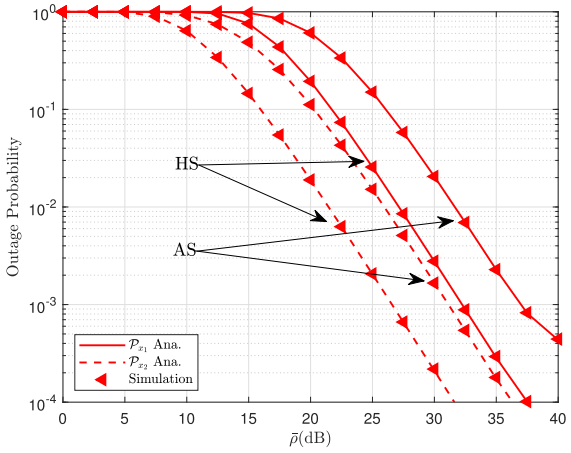

FIGURE 6. The outage probability versus $\bar{\rho}$, with different channel parameter of satellite link, where $\rho_S = 20dB$, $\rho_S = 5dB$ and $m = 2$.

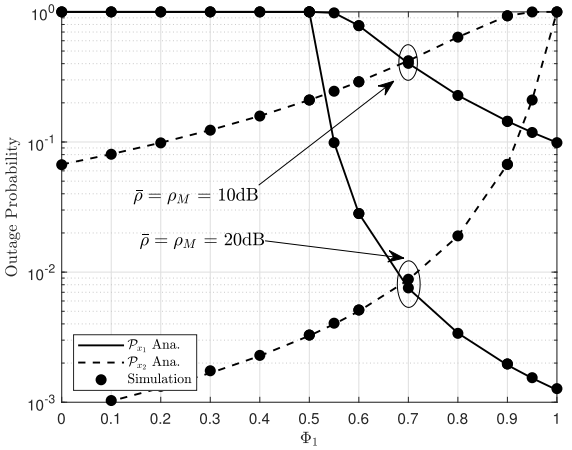

FIGURE 7. The outage probability versus Φ_1, with different values of $\bar{\rho} = \rho_M$, where $\rho_S = 5dB$, $m = 2$, $R_1 = R_2 = 0.5$ BPCU and the satellite link is set HS case.

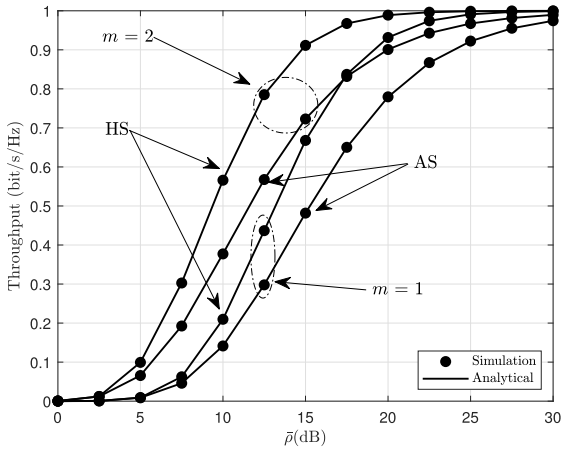

FIGURE 8. The throughput versus $\bar{\rho}$ with different channel parameter of satellite link and m, where $R_1 = R_2 = 0.5$ BPCU, $\rho_M = 20dB$ and $\rho_S = 5dB$.

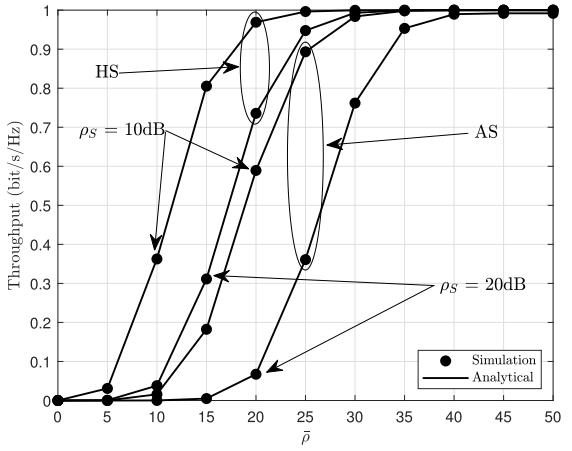

FIGURE 9. The throughput versus $\bar{\rho}$ with different channel parameter of satellite link and ρ_S, where $R_1 = R_2 = 0.5$ BPCU, $\rho_M = 20dB$ and $m = 2$.

rates lead to high throughput. When we increase $\bar{\rho}$ from 0 to 30, the throughput changes significantly. It is reported that the case of $m = 2$ and HS indicates the best throughput performance. The reason is that the throughput is computed based on the OPs. In similar viewpoint, Fig. 9 demonstrates

how the transmit SNRs ($\rho_S = 10$, and $\rho_S = 20$ make the influence to throughput.

V. CONCLUSION

In this paper, we have studied the operation of small cell to provide reliability transmission for HSTRS. Such system includes a geostationary satellite, two terrestrial users following the principle of NOMA scheme and terrestrial relays. We considered system performance of small-cell to reduce the impact of operations related to macro-cell users. Regarding the outage performance of HSTRS, we derived closed-form and asymptotic expressions of outage probability of two small-cell users. It was shown that the outage probability of HSTRS can be improved by increasing transmit power at base station. Moreover, the outage performance of HSTRS can be enhanced by employing the NOMA scheme compared to that using OMA scheme. In future work, multiple antennas and multiple users can be deployed in such HSTRS.

APPENDIX A

With the help (1) and (3), the first term A_1 can be written as (29), shown at the bottom of the page, in which $\rho_B = \frac{P_{SCB}}{N_0}$, $\bar{\rho}_B = \frac{\bar{P}_{SCB}}{N_0}$, $\rho_M = \frac{P_M}{N_0}$ and $\rho_S = \frac{P_{MCS}}{N_0}$.

Then, B_1 is rewritten as

$$\begin{aligned} B_1 &= \Pr\left(|h_{BR}|^2 > \frac{\theta_1\left(\rho_S|h_{MR}|^2+1\right)}{\bar{\rho}_B}, |h_{BM}|^2 < \frac{\rho_M}{\bar{\rho}_B}\right) \\ &= \underbrace{\Pr\left(|h_{BR}|^2 > \frac{\theta_1\left(\rho_S|h_{MR}|^2+1\right)}{\bar{\rho}_B}\right)}_{B_{1,1}} \underbrace{\Pr\left(|h_{BM}|^2 < \frac{\rho_M}{\bar{\rho}_B}\right)}_{B_{1,2}}. \end{aligned} \tag{30}$$

where $\theta_1 = \frac{\gamma_1}{\Phi_1 - \gamma_1\Phi_2}$.

Moreover, $B_{1,1}$ can be calculated by

$$\begin{aligned} B_{1,1} &= \Pr\left(|h_{BR}|^2 > \frac{\theta_1\left(\rho_S|h_{MR}|^2+1\right)}{\bar{\rho}_B}\right) \\ &= \int_0^\infty \bar{F}_{|h_{BR}|^2}\left(\frac{\theta_1(\rho_S z+1)}{\bar{\rho}_B}\right) f_{|h_{MR}|^2}(z)\,dz, \end{aligned} \tag{31}$$

where $\bar{F}_{|h|^2}(x) = 1 - F_{|h|^2}(x)$.

With the help of (10) and (13), we have

$$\begin{aligned} B_{1,1} = &\sum_{n_{MR}=0}^{m_{MR}-1} \zeta_{MR}(n_{MR}) \sum_{n_{BR}=0}^{m_{BR}-1}\sum_{a=0}^{n_{BR}} \binom{n_{BR}}{a} \\ &\times \frac{\alpha_{MR}\rho_S^a e^{-\frac{\theta_1}{\bar{\rho}_B\omega_{BR}}}}{\omega_{BR}^{n_{BR}} n_{BR}!} \left(\frac{\theta_1}{\bar{\rho}_B}\right)^{n_{BR}} \\ &\times \int_0^\infty z^{n_{MR}+a} e^{-\left(\frac{\theta_1\rho_S}{\bar{\rho}_B\omega_{BR}}+\Psi_{MR}\right)z} dz. \end{aligned} \tag{32}$$

Based on [37, Eq. 3.351.3], the closed-form of $B_{1,1}$ is obtained as

$$\begin{aligned} B_{1,1} = &\sum_{n_{MR}=0}^{m_{MR}-1}\sum_{n_{BR}=0}^{m_{BR}-1}\sum_{a=0}^{n_{BR}} \binom{n_{BR}}{a} \frac{\zeta_{MR}(n_{MR})(n_{MR}+a)!}{n_{BR}!} \\ &\times \frac{\alpha_{MR}\left(\omega_{BR}\bar{\rho}_B\right)^{n_{MR}-n_{BR}+a+1} e^{-\frac{\theta_1}{\bar{\rho}_B\omega_{BR}}}}{\rho_S^{-a}\theta_1^{-n_{BR}}\left(\theta_1\rho_S+\Psi_{MR}\bar{\rho}_B\omega_{BR}\right)^{n_{MR}+a+1}}. \end{aligned} \tag{33}$$

With the help of (13), $B_{1,2}$ is rewritten as

$$\begin{aligned} B_{1,2} &= \Pr\left(|h_{BM}|^2 < \frac{\rho_M}{\bar{\rho}_B}\right) \\ &= \frac{\gamma\left(m_{BM}, \rho_M/\omega_{BM}\bar{\rho}_B\right)}{\Gamma(m_{BM})}. \end{aligned} \tag{34}$$

Next, B_2 can be calculated by

$$\begin{aligned} B_2 &= \Pr\left(|h_{BR}|^2 > \frac{\theta_1|h_{BM}|^2\left(\rho_S|h_{MR}|^2+1\right)}{\rho_M}, |h_{BM}|^2 > \frac{\rho_M}{\bar{\rho}_B}\right) \\ &= \int_{\frac{\rho_M}{\bar{\rho}_B}}^\infty f_{|h_{BM}|^2}(x) \int_0^\infty f_{|h_{MR}|^2}(y) \\ &\quad \times \bar{F}_{|h_{BR}|^2}\left(\frac{\theta_1 x(\rho_S y+1)}{\rho_M}\right) dy dx. \end{aligned} \tag{35}$$

With the help (10), (11) and (12), we can rewrite (35) as

$$B_2 = \sum_{n_{MR}=0}^{m_{MR}-1}\sum_{n_{BR}=0}^{m_{BR}-1}\sum_{a=0}^{n_{BR}} \binom{n_{BR}}{a} \frac{\zeta_{MR}(n_{MR})}{\Gamma(m_{BM})}$$

$$\begin{aligned} A_1 &= \Pr\left(\frac{P_{SCB}|h_{BR}|^2\Phi_1}{P_{SCB}|h_{BR}|^2\Phi_2 + P_{MCS}|h_{MR}|^2 + N_0} > \gamma_1\right) \\ &= \underbrace{\Pr\left(\frac{\bar{\rho}_B|h_{BR}|^2\Phi_1}{\bar{\rho}_B|h_{BR}|^2\Phi_2 + \rho_S|h_{MR}|^2+1} > \gamma_1, \bar{\rho}_B < \frac{\rho_M}{|h_{BM}|^2}\right)}_{B_1} \\ &\quad + \underbrace{\Pr\left(\frac{\rho_M|h_{BR}|^2\Phi_1}{\rho_M|h_{BR}|^2\Phi_2 + |h_{BM}|^2\left(\rho_S|h_{MR}|^2+1\right)} > \gamma_1, \bar{\rho}_B > \frac{\rho_M}{|h_{BM}|^2}\right)}_{B_2}. \end{aligned} \tag{29}$$

$$\times \frac{(n_{MR}+a)!\alpha_{MR}\theta_1^{n_{BR}}(\rho_S)^a}{n_{BR}!(\rho_M\omega_{BR})^{n_{BR}}\omega_{BM}^{m_{BM}}} \times \int_0^\infty \frac{x^{m_{BM}+n_{BR}-1}e^{-\left(\frac{\theta_1}{\omega_{BR}\rho_M}+\frac{1}{\omega_{BM}}\right)x}\mathrm{H}\left(\frac{x\bar{\rho}_B}{\bar{\rho}_B}-1\right)}{\left(\frac{\theta_1\rho_S x}{\omega_{BR}\rho_M}+\Psi_{MR}\right)^{n_{MR}+a+1}}dx, \tag{36}$$

where H(.) denotes the Heaviside step function. Based on [34, Eq. 10], we have

$$(1+Px)^{-z} = \frac{1}{\Gamma(z)}G_{1,1}^{1,1}\left[Px\,\middle|\,\begin{matrix}1-z\\0\end{matrix}\right], \tag{37}$$

$$H(x-1) = G_{1,1}^{0,1}\left(x\,\middle|\,\begin{matrix}1\\0\end{matrix}\right), \tag{38}$$

where $G_{p,q}^{m,n}[.]$ is the Meijer's G-function [37, Eq. 9.301]. Then, we can rewrite B_2 as

$$B_2 = \sum_{n_{MR}=0}^{m_{MR}-1}\sum_{n_{BR}=0}^{m_{BR}-1}\sum_{a=0}^{n_{BR}}\binom{n_{BR}}{a}\frac{\zeta_{MR}(n_{MR})(n_{MR}+a)!}{n_{BR}!} \times \frac{\alpha_{MR}\theta_1^{n_{BR}}(\rho_S)^a(\Psi_{MR})^{-n_{MR}-a-1}}{\Gamma(n_{PR}+a+1)\Gamma(m_{BM})(\rho_M\omega_{BR})^{n_{BR}}\omega_{BM}^{m_{BM}}} \times \int_0^\infty x^{m_{BM}+n_{BR}-1}e^{-\frac{\theta_1\omega_{BM}+\omega_{BR}\rho_M}{\omega_{BR}\rho_M\omega_{BM}}x}G_{1,1}^{0,1}\left[\frac{x\bar{\rho}_B}{\rho_M}\,\middle|\,\begin{matrix}1\\0\end{matrix}\right] \times G_{1,1}^{1,1}\left[\frac{\theta_1\rho_S}{\omega_{BR}\rho_M\Psi_{MR}}x\,\middle|\,\begin{matrix}-n_{MR}-a\\0\end{matrix}\right]dx. \tag{39}$$

Following results in [36, Eq. 2.6.2], the inner integral of (39) is solved. Putting (33) and (34) into (30) then substituting the such result and (39) into (29), we can achieve final result. It completes the proof.

APPENDIX B

By using (1), the asymptotic of the CDF, i.e. $F^\infty_{\rho_B|h_{BR}|^2}(x)$ for peak interference constraint can be obtained as

$$F^\infty_{\rho_B|h_{BR}|^2}(x) = \int_0^{\frac{\rho_M}{\bar{\rho}_B}} F^\infty_{|h_{BR}|^2}\left(\frac{x}{\bar{\rho}_B}\right)f_{|h_{BM}|^2}(y)dy + \int_{\frac{\rho_M}{\bar{\rho}_B}}^\infty F^\infty_{|h_{BR}|^2}\left(\frac{xy}{\rho_M}\right)f_{|h_{BM}|^2}(y)dy. \tag{40}$$

With the help [37, Eq. 8.354.1], we can write

$$\gamma\left(m_i,\frac{x}{\omega_i}\right)\overset{x\to\infty}{\approx}\frac{1}{m_i}\left(\frac{x}{\omega_i}\right)^{m_i}. \tag{41}$$

Then, the asymptotic of $F_{|h_{BR}|^2}$ can be written as

$$F^\infty_{|h_BR|^2}(x) \approx \frac{1}{\Gamma(m_{BR}+1)}\left(\frac{x}{\omega_{BR}}\right)^{m_i}. \tag{42}$$

Next, we can obtain as

$$F^\infty_{\rho_B|h_{BR}|^2}(x) = \frac{\gamma\left(m_{BM},\frac{\rho_M}{\bar{\rho}_B\omega_{BM}}\right)}{\Gamma(m_{BR}+1)\Gamma(m_{BM})}\left(\frac{x}{\omega_{BR}\bar{\rho}_B}\right)^{m_{BR}} + \frac{\Gamma\left(m_{BM}+m_R,\frac{\rho_M}{\bar{\rho}_B\omega_{BM}}\right)}{\Gamma(m_{BR}+1)\Gamma(m_{BM})}\left(\frac{\omega_{BM}x}{\omega_{BR}\rho_M}\right)^{m_{BR}}. \tag{43}$$

$$\mathrm{A}_1^\infty = 1-\sum_{n_{MR}=0}^{m_{MR}-1}\sum_{n_{BR}=0}^{m_{BR}}\binom{m_{BR}}{n_{BR}}\frac{\zeta_{MR}(n_{MR})\rho_S^{n_{BR}}\alpha_{MR}(n_{MR}+n_{BR})!}{\Gamma(m_{BR}+1)\Gamma(m_{BM})\Psi_{MR}^{n_{MR}+n_{BR}+1}}\left(\frac{\theta_1}{\omega_{BR}}\right)^{m_{BR}} \times\left(\frac{\gamma\left(m_{BM},\frac{\rho_N}{\bar{\rho}_B\omega_{BM}}\right)}{\bar{\rho}_B^{m_{BR}}}+\Gamma\left(m_{SP}+m_R,\frac{\rho_M}{\bar{\rho}_B\omega_{BM}}\right)\left(\frac{\omega_{BM}}{\rho_M}\right)^{m_{BR}}\right). \tag{45}$$

$$A_2^\infty = 1-\sum_{n_{M1}=0}^{m_{M1}-1}\sum_{n_{R1}=0}^{m_{R1}}\binom{m_{R1}}{n_{R1}}\frac{\zeta_{M1}(n_{M1})\rho_S^{n_{R1}}\alpha_{M1}(n_{M1}+n_{R1})!}{\Gamma(m_{R1}+1)\Gamma(m_{RM})\Psi_{M1}^{n_{M1}+n_{R1}+1}}\left(\frac{\theta_1}{\omega_{R1}}\right)^{m_{R1}} \times\left(\frac{\gamma\left(m_{RM},\frac{\rho_M}{\bar{\rho}_R\omega_{RM}}\right)}{\bar{\rho}_R^{m_R}}+\Gamma\left(m_{RM}+m_{R1},\frac{\rho_M}{\bar{\rho}_R\omega_{RM}}\right)\left(\frac{\omega_{RM}}{\rho_M}\right)^{m_{R1}}\right). \tag{46}$$

$$A_3^\infty = 1-\sum_{n_{M2}=0}^{m_{M2}-1}\sum_{n_{R2}=0}^{m_{R2}}\binom{m_{R2}}{n_{R2}}\frac{\zeta_{M2}(n_{M2})\rho_S^{n_{R2}}\alpha_{M2}(n_{M2}+n_{R2})!}{\Gamma(m_{R2}+1)\Gamma(m_{RM})\Psi_{M2}^{n_{M2}+n_{R2}+1}}\left(\frac{\theta_1}{\omega_{R2}}\right)^{m_{R2}} \times\left(\frac{\gamma\left(m_{RM},\frac{\rho_M}{\bar{\rho}_R\omega_{RM}}\right)}{\bar{\rho}_R^{m_R}}+\Gamma\left(m_{RM}+m_{R2},\frac{\rho_M}{\bar{\rho}_R\omega_{RM}}\right)\left(\frac{\omega_{RM}}{\rho_M}\right)^{m_{R2}}\right). \tag{47}$$

Thus, A_1^{∞} can be calculated as

$$A_1^{\infty} = \Pr\left(\rho_B |h_{BR}|^2 > \theta_1 \left(\rho_S |h_{MR}|^2 + 1\right)\right) = 1 - \int_0^{\infty} \left(F^{\infty}_{\rho_B|h_{BR}|^2}\left(\theta_1\left(\rho_P y + 1\right)\right)\right) f_{|h_{MR}|^2}(y)\, dy. \quad (44)$$

It is noted that the asymptotic of A_2^{∞} and A_3^{∞} can be obtained as (46), (47), shown at the bottom of the previous page, respectively.

Now, using (45), (46) and (47), the result in (25) can be attained.

This completes the proof.

REFERENCES

[1] B. Evans, M. Werner, E. Lutz, M. Bousquet, G. E. Corazza, G. Maral, and R. Rumeau, "Integration of satellite and terrestrial systems in future multimedia communications," *IEEE Wireless Commun.*, vol. 12, no. 5, pp. 72–80, Oct. 2005.

[2] G. Zheng, S. Chatzinotas, and B. Ottersten, "Generic optimization of linear precoding in multibeam satellite systems," *IEEE Trans. Wireless Commun.*, vol. 11, no. 6, pp. 2308–2320, Jun. 2012.

[3] A. Vanelli-Corali, G. E. Corazza, G. K. Karagiannidis, P. T. Mathiopoulos, D. S. Michalopoulos, C. Mosquera, S. Papaharalabos, and S. Scalise, "Satellite communications: Research trends and open issues," in *Proc. Int. Workshop Satell. Space Commun.*, Salzburg, Austria, Sep. 2007, pp. 71–75.

[4] M. R. Bhatnagar and M. K. Arti, "Performance analysis of AF based hybrid satellite-terrestrial cooperative network over generalized fading channels," *IEEE Commun. Lett.*, vol. 17, no. 10, pp. 1912–1915, Oct. 2013.

[5] V. K. Sakarellos, C. Kourogiorgas, and A. D. Panagopoulos, "Cooperative hybrid land mobile satellite–terrestrial broadcasting systems: Outage probability evaluation and accurate simulation," *Wireless Pers. Commun.*, vol. 79, no. 2, pp. 1471–1481, Nov. 2014.

[6] M. K. Arti and V. Jain, "Relay selection-based hybrid satellite-terrestrial communication systems," *IET Commun.*, vol. 11, no. 17, pp. 2566–2574, Nov. 2017.

[7] S. Sreng, B. Escrig, and M.-L. Boucheret, "Exact outage probability of a hybrid satellite terrestrial cooperative system with best relay selection," in *Proc. IEEE Int. Conf. Commun. (ICC)*, Budapest, Hungary, Jun. 2013, pp. 4520–4524.

[8] K. An, M. Lin, J. Ouyang, Y. Huang, and G. Zheng, "Symbol error analysis of hybrid satellite–terrestrial cooperative networks with cochannel interference," *IEEE Commun. Lett.*, vol. 18, no. 11, pp. 1947–1950, Nov. 2014.

[9] H. Wu, Y. Zou, W. Cao, Z. Chen, T. A. Tsiftsis, M. R. Bhatnagar, and R. C. De Lamare, "Impact of hardware impairments on outage performance of hybrid satellite-terrestrial relay systems," *IEEE Access*, vol. 7, pp. 35103–35112, 2019.

[10] R. Wang, F. Zhou, J. Bian, K. An, and K. Guo, "Performance evaluation of HARQ-assisted hybrid satellite-terrestrial relay networks," *IEEE Commun. Lett.*, vol. 24, no. 2, pp. 423–427, Feb. 2020.

[11] P. K. Sharma, D. Deepthi, and D. I. Kim, "Outage probability of 3-D mobile UAV relaying for hybrid satellite-terrestrial networks," *IEEE Commun. Lett.*, vol. 24, no. 2, pp. 418–422, Feb. 2020.

[12] Y. Zou, J. Zhu, X. Wang, and L. Hanzo, "A survey on wireless security: Technical challenges, recent advances, and future trends," *Proc. IEEE*, vol. 104, no. 9, pp. 1727–1765, Sep. 2016.

[13] D.-T. Do and A.-T. Le, "NOMA based cognitive relaying: Transceiver hardware impairments, relay selection policies and outage performance comparison," *Comput. Commun.*, vol. 146, pp. 144–154, Oct. 2019.

[14] T.-L. Nguyen and D.-T. Do, "Power allocation schemes for wireless powered NOMA systems with imperfect CSI: An application in multiple antenna-based relay," *Int. J. Commun. Syst.*, vol. 31, no. 15, p. e3789, Oct. 2018.

[15] D.-T. Do, A.-T. Le, and B. M. Lee, "NOMA in cooperative underlay cognitive radio networks under imperfect SIC," *IEEE Access*, vol. 8, pp. 86180–86195, 2020.

[16] X. Li, M. Zhao, Y. Liu, L. Li, Z. Ding, and A. Nallanathan, "Secrecy analysis of ambient backscatter NOMA systems under I/Q imbalance," *IEEE Trans. Veh. Technol.*, early access, Jul. 2, 2020, doi: 10.1109/TVT.2020.3006478.

[17] X. Li, Q. Wang, H. Peng, H. Zhang, D.-T. Do, K. M. Rabie, R. Kharel, and C. C. Cavalcante, "A unified framework for HS-UAV NOMA networks: Performance analysis and location optimization," *IEEE Access*, vol. 8, pp. 13329–13340, 2020, doi: 10.1109/ACCESS.2020.2964730.

[18] X. Li, Q. Wang, Y. Liu, T. A. Tsiftsis, Z. Ding, and A. Nallanathan, "UAV-aided multi-way NOMA networks with residual hardware impairments," *IEEE Wireless Commun. Lett.*, vol. 9, no. 9, pp. 1538–1542, Sep. 2020.

[19] X. Yan, H. Xiao, C.-X. Wang, and K. An, "Outage performance of NOMA-based hybrid satellite-terrestrial relay networks," *IEEE Wireless Commun. Lett.*, vol. 7, no. 4, pp. 538–541, Aug. 2018.

[20] X. Yan, H. Xiao, K. An, G. Zheng, and W. Tao, "Hybrid satellite terrestrial relay networks with cooperative non-orthogonal multiple access," *IEEE Commun. Lett.*, vol. 22, no. 5, pp. 978–981, May 2018.

[21] X. Yan, H. Xiao, C.-X. Wang, and K. An, "On the ergodic capacity of NOMA-based cognitive hybrid satellite terrestrial networks," in *Proc. IEEE/CIC Int. Conf. Commun. China (ICCC)*, Oct. 2017, pp. 1–5.

[22] X. Yan, K. An, T. Liang, G. Zheng, and Z. Feng, "Effect of imperfect channel estimation on the performance of cognitive satellite terrestrial networks," *IEEE Access*, vol. 7, pp. 126293–126304, 2019.

[23] V. Singh, V. Bankey, and P. K. Upadhyay, "Underlay cognitive hybrid satellite-terrestrial networks with cooperative-NOMA," in *Proc. IEEE Wireless Commun. Netw. Conf. (WCNC)*, Seoul, South Korea, May 2020, pp. 1–6.

[24] R. Madan, J. Borran, A. Sampath, N. Bhushan, A. Khandekar, and T. Ji, "Cell association and interference coordination in heterogeneous LTE—A cellular networks," *IEEE J. Sel. Areas Commun.*, vol. 28, no. 9, pp. 1479–1489, Dec. 2010.

[25] S. Singh and J. G. Andrews, "Joint resource partitioning and offloading in heterogeneous cellular networks," *IEEE Trans. Wireless Commun.*, vol. 13, no. 2, pp. 888–901, Feb. 2014.

[26] J. G. Andrews, "Seven ways that HetNets are a cellular paradigm shift," *IEEE Commun. Mag.*, vol. 51, no. 3, pp. 136–144, Mar. 2013.

[27] Z. Tan, X. Li, F. R. Yu, H. Ji, and V. C. M. Leung, "Joint resource allocation in cache-enabled small cell networks with massive MIMO and full duplex," in *Proc. IEEE Global Commun. Conf. (GLOBECOM)*, Singapore, Dec. 2017, pp. 1–6.

[28] D.-T. Do, C.-B. Le, and F. Afghah, "Enabling full-duplex and energy harvesting in uplink and downlink of small-cell network relying on power domain based multiple access," *IEEE Access*, vol. 8, pp. 142772–142784, 2020.

[29] H. Liu and K. S. Kwak, "Opportunistic relaying for cooperative small-cell systems with unreliable wireless backhauls," in *Proc. IEEE Wireless Commun. Netw. Conf. (WCNC)*, Barcelona, Spain, Apr. 2018, pp. 1–6.

[30] B. Yafis, K.-T. Feng, and C.-M. Yu, "Renewable energy-based resource allocation for full-duplex small cell networks," *IEEE Access*, vol. 6, pp. 24746–24756, 2018.

[31] H. Zhang, Y. Wang, H. Ji, and X. Li, "A sleeping mechanism for cache-enabled small cell networks with energy harvesting function," *IEEE Trans. Green Commun. Netw.*, vol. 4, no. 2, pp. 497–505, Jun. 2020.

[32] A. Haider and S.-H. Hwang, "Maximum transmit power for UE in an LTE small cell uplink," *Electronics*, vol. 8, no. 7, p. 796, Jul. 2019.

[33] N. I. Miridakis, D. D. Vergados, and A. Michalas, "Dual-hop communication over a satellite relay and shadowed Rician channels," *IEEE Trans. Veh. Technol.*, vol. 64, no. 9, pp. 4031–4040, Sep. 2015.

[34] V. S. Adamchik and O. I. Marichev, "The algorithm for calculating integrals of hypergeometric type functions and its realization in REDUCE system," in *Proc. Int. Symp. Symbolic Algebr. Comput. (ISSAC)*, Tokyo, Japan, 1990, pp. 212–224.

[35] A. Abdi, W. C. Lau, M. Alouini, and M. Kaveh, "A new simple model for land mobile satellite channels: First- and second-order statistics," *IEEE Trans. Wireless Commun.*, vol. 2, no. 3, pp. 519–528, May 2003.

[36] A. M. Mathai and R. K. Saxena *The H-Function With Applications in Statistics and Other Disciplines*. Hoboken, NJ, USA: Wiley, 1978.

[37] I. S. Gradshteyn and I. M. Ryzhik, *Table of Integrals, Series, and Products*, 6th ed. San Diego, CA, USA: Academic, 2000.

NGOC-LONG NGUYEN was born in Binh Dinh, Vietnam, in August 1973. He received the B.S. and M.S. degrees in electric physics from the University of Science, Vietnam. He is currently pursuing the Ph.D. degree with the VSB Technical University of Ostrava, Czech Republic. He is also working as a Lecturer with the Faculty of Applied Sciences, Ton Duc Thang University. His research interests include applied electronics, satellite systems, non-orthogonal multiple access, and energy harvesting.

HONG-NHU NGUYEN was born in Tien Giang, Vietnam, in March 1971. He received the B.Sc. degree in electronics engineering from the Ho Chi Minh City University of Technology, in 1998, and the M.Sc. degree in electronics engineering from the University of Transport and Communications, Vietnam, in 2012. He is currently pursuing the Ph.D. degree with the VSB Technical University of Ostrava, Czech Republic. He is also working as a Lecturer with Sai Gon University. His research interests include applied electronics, wireless communication, cognitive radio, and energy harvesting.

ANH-TU LE was born in Lam Dong, Vietnam, in 1997. He is currently pursuing the master's degree in communication and information system fin field of wireless communication. He is also a Research Assistant with the Industrial University of Ho Chi Minh City, Vietnam. He has authored or coauthored over 15 technical articles published in peer-reviewed international journals. His research interests include wireless channel modelling, NOMA, cognitive radio, and MIMO.

DINH-THUAN DO (Senior Member, IEEE) received the B.S., M.Eng., and Ph.D. degrees in communications engineering from Viet Nam National University (VNU-HCMC), in 2003, 2007, and 2013, respectively. From 2003 to 2009, he was a Senior Engineer with VinaPhone Mobile Network. From 2009 to 2010, he was a Visiting Ph.D. Student with the Communications Engineering Institute, National Tsing Hua University, Taiwan. He published one book and one book chapter. He has authored or coauthored over 75 technical articles published in peer-reviewed international journals (SCIE) and over 60 conference papers. His research interests include signal processing in wireless communications networks, MIMO, NOMA, UAV networks, satellite systems, physical layer security, device-to-device transmission, and energy harvesting. He was a recipient of the Golden Globe Award from Vietnam Ministry of Science and Technology, in 2015 (Top 10 talent young scientist in Vietnam). He received the Creative Young Medal, in 2015. He led as a Lead Guest Editor in several special issues in peer-reviewed journals. He serves as an Associate Editor for six ISI/Scopus journals.

MIROSLAV VOZNAK (Senior Member, IEEE) received the Ph.D. degree in telecommunications from the Faculty of Electrical Engineering and Computer Science, VSB-Technical University of Ostrava, in 2002, and the Habilitation degree, in 2009. He was appointed as a Full Professor of electronics and communications technologies, in 2017. He is the author or coauthor of more than 100 articles in SCI/SCIE journals. His research interests include information and communication technologies, especially on quality of service and experience, network security, wireless networks, and big data analytics. He has served as a member of editorial boards for several journals, including *Sensors*, the *Journal of Communications*, *Elektronika Ir Elektrotechnika*, and *Advances in Electrical and Electronic Engineering*.